Tracking and convergence of multi-channel Kalman filters for active noise control

Arthur Berkhoff[1,2] and Sjoerd van Ophem[2]
[1]TNO Technical Sciences, Acoustics and Sonar, The Hague, The Netherlands, *
[2]University of Twente, Faculty EEMCS, Enschede, The Netherlands, †

ABSTRACT

The feed-forward broadband active noise control problem can be formulated as a state estimation problem to achieve a faster rate of convergence than the filtered reference least mean squares algorithm and possibly also a better tracking performance. A multiple input/multiple output Kalman algorithm is used to perform this state estimation. To make the algorithm more suitable for real-time applications the Kalman filter is written in a fast array form and the secondary path state matrices are implemented in output normal form. The implementation was tested in simulations and in real-time experiments. It was found that for a constant primary path the Kalman filter has a fast rate of convergence and is able to track changes in the spectrum. For a forgetting factor equal to unity the system is robust, but the filter is unable to track rapid changes in the primary path. It is shown that a forgetting factor lower than unity gives a significantly improved tracking performance. Numerical issues of the fast array form of the algorithm for such forgetting factors are discussed and possible solutions are presented.

1. Introduction

Filtered-reference and filtered-error least means squares algorithms based on approximate, instantaneous gradients are widely used for adapting an Active Noise Control (ANC) system. The algorithms are relatively simple and robust, but one of the biggest drawbacks of the algorithms are the low rate of convergence leading to slow adaption to changes in the primary path. The assumption that is used is that the filter coefficients are changing slowly in comparison to the timescale of the plant dynamics, see Elliott [1]. Several approaches have been suggested to improve the speed of convergence of least-mean-square based algorithms, such as the modified fx-LMS algorithm proposed by Bjarnason [2], Fast Affine Projections, Preconditioned LMS [1] and other methods.

Recursive Least Squares (RLS) algorithms have a faster rate of convergence, but require more computational effort. A modified RLS algorithm has been derived by Flockton [3], which has a similar structure as a modified LMS-algorithm. The disadvantages of this algorithm are the initial overshoot when the filter is turned on and slow tracking behavior. Sayed *et al.* [4] have shown that the RLS filter

*arthur.berkhoff@tno.nl
†a.p.berkhoff@utwente.nl

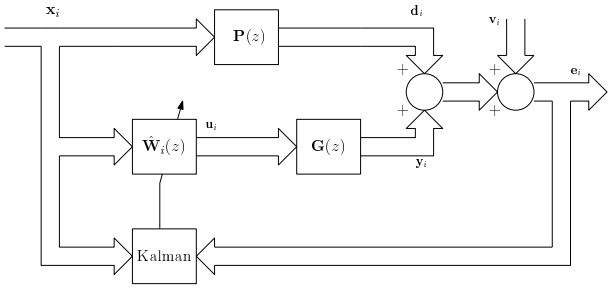

Figure 1: Block diagram of a MIMO ANC system with a Kalman filter.

is a special case of a Kalman filter. A SISO Kalman filter was described by Fraanje [5] in an ANC context, in which it was shown that there is no initial overshoot before convergence when a properly tuned Kalman filter is used for an ANC application. This filter estimates the state of the secondary path and the filter coefficients and takes uncertainty of the state and uncertainty in measurements into account, which explains the abscence of the overshoot in the convergence curve. As compared to the RLS filter, tracking behavior is potentially improved because system uncertainties are taken into account in the algorithm.

This paper shows results of a multiple input multiple output Kalman filter as derived for an ANC system [6, 7]. This algorithm includes an extension with a state space description of the secondary path in output normal form. This requires less computational effort and is numerically more robust. Simulations will be shown of a multiple input multiple output implementation of the Kalman recursions in free field conditions. The performance of the algorithm was tested in a real-time experiment in which the goal was to minimize the noise at the end of a duct for time-varying signals. The first part of this paper is based on Ref. [6], while the second part is based on [7].

2. MIMO Kalman filter

2.1 Model description

Consider an ANC system which has N_x reference channels, N_u control channels and N_e error channels with the reference signal vector $\mathbf{x}(i) \in \mathbb{R}^{N_x}$, the control signal vector $\mathbf{u}(i) \in \mathbb{R}^{N_u}$, and the error signal vector $\mathbf{e}(i) \in \mathbb{R}^{N_e}$, in which i is the time instance. In this paper, the time index i is indicated either as a subscript or between parentheses. It is assumed that there is no feedback from the actuators to the reference microphones, so the control system can be seen as a purely feed-forward system, as shown in Fig. 1. In this figure $\mathbf{P}(z)$ represents the primary path from the reference microphone to the error microphone, $\mathbf{G}(z)$ represents the secondary path from the secondary actuator to the error microphone and $\hat{\mathbf{W}}_{i,\mathrm{FIR}}(z)$ is the controller, adapted by a Kalman filter.

The adaptive controller has a feed-forward structure and is described by the matrix $\hat{\mathbf{W}}_{i,\mathrm{FIR}}(z) \in \mathbb{R}^{N_u \times N_x}$ consisting of FIR-filters with n_w filter coefficients. The $(k,l)_{th}$ term of this matrix, with $0 \leq k \leq N_u,\ 0 \leq l \leq N_x$ can be described by:

$$\hat{\mathbf{W}}^{(k,l)}_{i,\mathrm{FIR}}(z) = \hat{w}^{(k,l)}_0(i) + \hat{w}^{(k,l)}_1(i)z^{-1} + ...\hat{w}^{(k,l)}_{n_w-1}(i)z^{-n_w-1}. \tag{1}$$

The individual filter coefficients can be organized as follows:

$$\hat{\mathbf{w}}^{(k,l)}(i) = \left[\ \hat{w}^{(k,l)}_0(i) \quad ... \quad \hat{w}^{(k,l)}_{n_w-1}(i)\ \right]^T \in \mathbb{R}^{n_w \times 1}, \tag{2}$$

$$\hat{\mathbf{w}}^{(k)}(i) = \left[\ \hat{\mathbf{w}}^{(k,1)}(i)^T \quad ... \quad \hat{\mathbf{w}}^{(k,N_x)}(i)^T\ \right]^T \in \mathbb{R}^{n_w N_x \times 1}, \tag{3}$$

$$\hat{\mathbf{W}}(i) = \left[\ \hat{\mathbf{w}}^{(1)}(i) \quad ... \quad \hat{\mathbf{w}}^{(N_u)}(i)\ \right] \in \mathbb{R}^{n_w N_x \times N_u}. \tag{4}$$

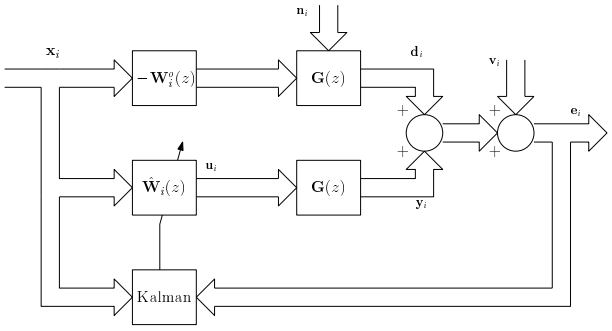

Figure 2: Block diagram of a MIMO ANC system with an approximate representation of the primary path.

$$\hat{\mathbf{w}}^{(k)}(i) = \left[\begin{array}{ccc} \hat{\mathbf{w}}^{(k,1)}(i)^T & \ldots & \hat{\mathbf{w}}^{(k,N_x)}(i)^T \end{array} \right]^T \in \mathbb{R}^{n_w N_x \times 1}, \tag{5}$$

The N_x vectors with the last n_w steps of the n_x-th reference signal $\mathbf{x}_{n_w}^{n_x}(i)$ are stacked in the vector $\mathbf{x}_{n_w}(i)$. The resulting control signals are (using $\mathrm{vec}(\mathbf{ABC}) = (\mathbf{C}^T \otimes \mathbf{A})\mathrm{vec}(\mathbf{B})$ [8]):

$$\begin{aligned} \mathbf{u}(i) &= -\hat{\mathbf{W}}^T(i)\mathbf{x}_{n_w}(i) = -\mathrm{vec}(\mathbf{x}_{n_w}^T(i)\hat{\mathbf{W}}(i)I_{N_u}) \\ &= -(\boldsymbol{I}_{N_u} \otimes \mathbf{x}_{n_w}^T(i))\hat{\mathbf{w}}(i). \end{aligned} \tag{6}$$

In this equation $\boldsymbol{I}_{N_u}$ is the identity matrix of size N_u. When the controller reaches its optimal value $\mathbf{w}^o(i)$, the control signal vector is:

$$\mathbf{u}^o(i) = -(\boldsymbol{I}_{N_u} \otimes \mathbf{x}_{n_w}^T(i))\mathbf{w}^o(i). \tag{7}$$

2.2 Augmented state space description

The MIMO ANC problem is written in a state space form, where the purpose of the FIR controller is to minimize the error $\mathbf{e}(i) = \mathbf{d}(i) + \mathbf{y}(i) + \mathbf{v}(i)$, in which $\mathbf{d}(i)$ is the influence of the primary paths on the error microphones, $\mathbf{y}(i)$ is the influence of the secondary path on the error sensors and $\mathbf{v}_i$ is assumed to be a Gaussian white noise signal vector, corrupting the measurement of the error sensors. The error is minimized when the FIR filters are adjusted to their optimal values $\mathbf{W}_i^o(z)$, so that $\mathbf{d}(i) = -\mathbf{y}(i)$. As stated by Sayyarrodsari [9] the purpose of the active noise control algorithm is to make a model of the primary path with the series connection of the FIR filter matrix and the secondary path. Therefore the primary path can be approximated by a series connection of the optimal filter $-\mathbf{W}_i^o(z)$ and the secondary path $\mathbf{G}(z)$, as shown in Fig. 2. A noise vector $\mathbf{n}(i)$ is included to account for modeling uncertainties. Using the methods of [10] and defining the augmented state vector

$$\boldsymbol{\chi}(i) = \left[\begin{array}{c} \mathbf{w}(i) \\ \boldsymbol{\theta}(i) \end{array} \right], \tag{8}$$

the augmented state space description can be written as:

$$\begin{aligned} \left[\begin{array}{c} \mathbf{w}(i+1) \\ \boldsymbol{\theta}(i+1) \end{array} \right] &= \boldsymbol{A}(i) \left[\begin{array}{c} \mathbf{w}(i) \\ \boldsymbol{\theta}(i) \end{array} \right] - \boldsymbol{B}(i)\hat{\mathbf{w}}(i) + \boldsymbol{H}(i)\mathbf{n}(i)\ , \\ \mathbf{e}(i) &= \boldsymbol{C}(i) \left[\begin{array}{c} \mathbf{w}(i) \\ \boldsymbol{\theta}(i) \end{array} \right] - \boldsymbol{D}(i)\hat{\mathbf{w}}(i) + \mathbf{v}(i), \ \left[\begin{array}{c} \mathbf{w}(0) \\ \boldsymbol{\theta}(0) \end{array} \right] = \left[\begin{array}{c} \mathbf{w}^o(0) \\ \boldsymbol{\theta}(0) \end{array} \right] \end{aligned} \tag{9}$$

Introducing a forgetting factor $0 \ll \lambda \leq 1$ [10], the full state space description for a MIMO ANC feed-forward system can be written as:

$$
\begin{aligned}
\mathbf{A}(i) &= \begin{bmatrix} \lambda^{-1/2}\boldsymbol{I}_{n_w N_u N_x} & \mathbf{0}_{n_w N_u N_x \times n_s} \\ \mathbf{B}_s(\boldsymbol{I}_{N_u} \otimes \mathbf{x}_{n_w}^T(i)) & \mathbf{A}_s \end{bmatrix}, && (10)\\
\mathbf{B}(i) &= \begin{bmatrix} \mathbf{0}_{n_w N_u N_x \times n_w N_u N_x} \\ -\mathbf{B}_s(\boldsymbol{I}_{N_u} \otimes \mathbf{x}_{n_w}^T(i)) \end{bmatrix}, && (11)\\
\mathbf{C}(i) &= \begin{bmatrix} \mathbf{D}_s(\boldsymbol{I}_{N_u} \otimes \mathbf{x}_{n_w}^T(i)) & \mathbf{C}_s \end{bmatrix}, && (12)\\
\mathbf{D}(i) &= -\mathbf{D}_s(\boldsymbol{I}_{N_u} \otimes \mathbf{x}_{n_w}^T(i)), && (13)\\
\mathbf{H} &= \begin{bmatrix} \mathbf{0}_{n_w N_u N_x \times N_e N_x} \\ \mathbf{H}_s \end{bmatrix}, && (14)
\end{aligned}
$$

leading to the state space description

$$
\begin{aligned}
\boldsymbol{\chi}(i+1) &= \mathbf{A}(i)\boldsymbol{\chi}(i) + \mathbf{B}(i)\hat{\mathbf{w}}(i) + \mathbf{H}\mathbf{n}(i),\\
\mathbf{e}(i) &= \mathbf{C}(i)\boldsymbol{\chi}(i) + \mathbf{D}(i)\hat{\mathbf{w}}(i) + \mathbf{v}(i). && (15)
\end{aligned}
$$

2.3 Kalman filtering

To estimate the state of the ANC system a Kalman filter is used, in which the Kalman filter explicitly takes the covariances from the noise vectors $\mathbf{n}_i$ and $\mathbf{v}_i$ into account and gives a minimum variance estimate of the state. The initial state is assumed to be uncorrelated with the noise terms $\mathbf{n}_i$ and $\mathbf{v}_i$. Also the inididual noise terms are assumed to be uncorrelated, resulting in

$$
\mathrm{E}\left(\begin{bmatrix} \boldsymbol{\chi}(0) \\ \mathbf{n}(0) \\ \mathbf{v}(0) \end{bmatrix} \begin{bmatrix} \boldsymbol{\chi}(0) \\ \mathbf{n}(0) \\ \mathbf{v}(0) \end{bmatrix}^T \right) = \begin{bmatrix} \boldsymbol{\Pi}(0) & \mathbf{0} & \mathbf{0} \\ \mathbf{0} & \mathbf{Q}\delta_{kl} & \mathbf{0} \\ \mathbf{0} & \mathbf{0} & \mathbf{R}\delta_{kl} \end{bmatrix}. \qquad (16)
$$

In this equation δ_{ij} is the Dirac delta function and $\boldsymbol{\Pi}(0)$ is called the state covariance matrix, defined as

$$
\boldsymbol{\Pi}(0) = \begin{bmatrix} \boldsymbol{\Pi}^{ww}(0) & \boldsymbol{\Pi}^{w\theta}(0) \\ \boldsymbol{\Pi}^{\theta w}(0) & \boldsymbol{\Pi}^{\theta\theta}(0) \end{bmatrix}, \qquad (17)
$$

with $\boldsymbol{\Pi}_0^{ww} = \mathrm{E}[\mathbf{w}(0)\mathbf{w}^T(0)],\ \boldsymbol{\Pi}_0^{w\theta} = \boldsymbol{\Pi}_0^{\theta w^T} = \mathrm{E}[\mathbf{w}(0)\boldsymbol{\theta}^T(0)],\ \Pi_0^{\theta\theta} = \mathrm{E}[\boldsymbol{\theta}(0)\boldsymbol{\theta}^{\mathrm{T}}(0)]$.
Furthermore $\mathbf{Q}$ and $\mathbf{R}$ are the noise covariance matrices, and are given by

$$
\begin{aligned}
\mathbf{Q} &= \begin{bmatrix} Q_{11} & \cdots & 0 \\ \vdots & \ddots & \vdots \\ 0 & \cdots & Q_{N_x N_e} \end{bmatrix}, && (18)\\
\mathbf{R} &= \begin{bmatrix} R_1 & \cdots & 0 \\ \vdots & \ddots & \vdots \\ 0 & \cdots & R_{N_e} \end{bmatrix}. && (19)
\end{aligned}
$$

The estimate of the control coefficients $\hat{\mathbf{w}}(i)$ and the estimate of the state vector $\hat{\boldsymbol{\theta}}(i)$ are combined in the estimate of the augmented state vector

$$
\hat{\boldsymbol{\chi}}(i) = \begin{bmatrix} \hat{\mathbf{w}}(i) \\ \hat{\boldsymbol{\theta}}(i) \end{bmatrix}, \qquad (20)
$$

Then the MIMO Kalman filter in covariance form is given by the following equations:

$$
\begin{aligned}
\hat{\boldsymbol{\chi}}(0) &= \mathbf{0}_{n_w N_u N_x + n_s \times 1}, && (21)\\
\mathbf{P}(0) &= \boldsymbol{\Pi}(0), && (22)\\
\boldsymbol{\epsilon}(i) &= \mathbf{e}(i) - \mathbf{C}_s \hat{\boldsymbol{\chi}}(i) - \mathbf{D}_s \hat{\mathbf{w}}(i), && (23)\\
\mathbf{R}_e(i) &= \mathbf{R} + \mathbf{C}(i)\mathbf{P}(i)\mathbf{C}^T(i), && (24)\\
\mathbf{K}(i) &= \mathbf{A}(i)\mathbf{P}(i)\mathbf{C}^T(i), && (25)\\
\hat{\boldsymbol{\chi}}(i+1) &= \mathbf{A}_s \hat{\boldsymbol{\chi}}(i) + \mathbf{B}_s \hat{\mathbf{w}}(i) + \mathbf{K}(i)\mathbf{R}_e^{-1}(i)\boldsymbol{\epsilon}(i) && (26)\\
\mathbf{P}(i+1) &= \mathbf{A}(i)\mathbf{P}(i)\mathbf{A}^T(i) - \mathbf{K}(i)\mathbf{R}_e^{-1}(i)\mathbf{K}^T(i) + \mathbf{H}\mathbf{Q}\mathbf{H}^T. && (27)
\end{aligned}
$$

For a derivation of these equations, see Sayed [11]. In these equations $\mathbf{P}(i)$ represents the covariance matrix of the state estimation error, $\boldsymbol{\epsilon}(i)$ the innovation vector, $\mathbf{R}_e(i)$ the error covariance matrix and $\mathbf{K}(i)$ the gain matrix. Since the state is augmented, some of these expressions can be reduced and partitioned as follows:

$$
\begin{aligned}
\mathbf{P}(i) &= \begin{bmatrix} \mathbf{P}^{ww}(i) & \mathbf{P}^{w\theta}(i) \\ \mathbf{P}^{\theta w}(i) & \mathbf{P}^{\theta\theta}(i) \end{bmatrix}, && (28)\\
\mathbf{K}(i) &= \begin{bmatrix} \mathbf{K}^{w}(i) \\ \mathbf{K}^{\theta}(i) \end{bmatrix}, \\
\boldsymbol{\epsilon}(i) &= \mathbf{e}(i) - \mathbf{C}_s \hat{\boldsymbol{\theta}}(i), && (29)\\
\begin{bmatrix} \hat{\mathbf{w}}(i+1) \\ \hat{\boldsymbol{\theta}}(i+1) \end{bmatrix} &= \begin{bmatrix} \lambda^{-1/2}\hat{\mathbf{w}}(i) \\ \mathbf{A}_s \hat{\boldsymbol{\theta}}(i) \end{bmatrix} + \begin{bmatrix} \mathbf{K}^{w}(i) \\ \mathbf{K}^{\theta}(i) \end{bmatrix} \mathbf{R}_e^{-1}(i)\boldsymbol{\epsilon}(i), && (30)
\end{aligned}
$$

in which $\mathbf{K}_i^w \in \mathbb{R}^{n_w N_u N_x \times N_e}$, and $\mathbf{K}_i^\theta \in \mathbb{R}^{n_s \times N_e}$. The straightforward implementation of Eqs. (21) - (27) gives a computationally demanding algorithm. A more efficient algorithm can be achieved by making use of the shift-invariance of the reference signals. Use of shift invariance properties, the resulting Fast Array descriptions, and a specific initialization leading to a reduced rank of the update scheme, are summarized in Ref. [10].

3. Output normal form parameterization

The state space description of the secondary path is rewritten to an output normal form parameterization. This parameterization has a few advantages in comparison to the full state space model. As shown in Ref. [12], not only the calculations needed to do the multiplications with the state matrices reduce due to the Hessenberg form of the state matrix, but the parameterization also makes it possible to solve the multiplications in a recursive way, leading to even more reduction of the floating point operations needed. Another benefit of the state space parameterization is the reduction of redundancy in the state matrices.

3.1 Transformation to output normal form

When the assumption that the secondary path doesn't change in time is met, the state matrices can be identified off-line. After identification the states can be transformed if the states are observable. An output norm form transforms the state matrices in such a way the observability Gramian is the identity matrix:

$$
A_s^T A_s + C_s^T C_s = I. \tag{31}
$$

When this is true, the states are orthogonal, giving several numerical advantages in comparison to the full state space model, in which the most important are the low round off noise gain and the notion

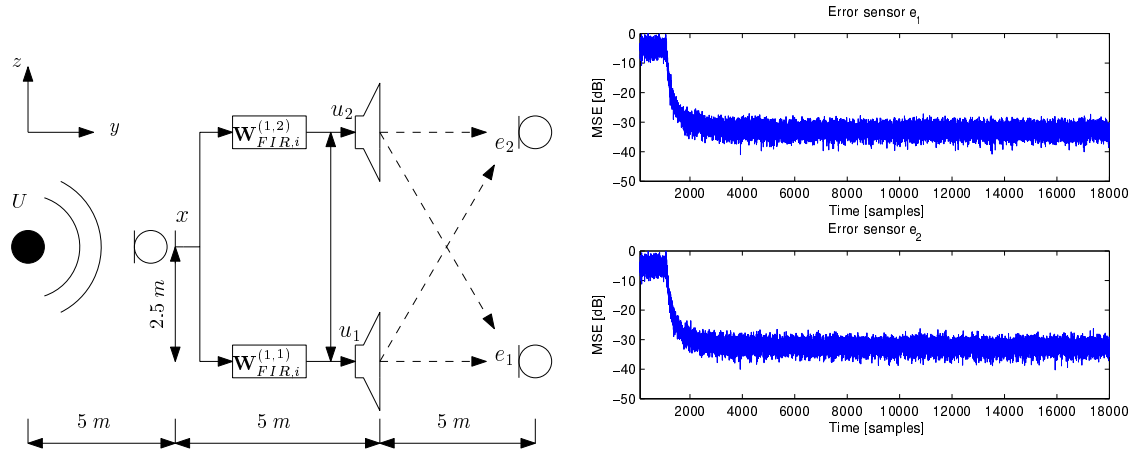

Figure 3: MIMO setup (left) and mean squared signal at the error sensors (right); filter turned on after 1000 samples, average of 50 simulations.

that the amplitude of the signal is not changed throughout the filter (Roberts *et al.* [13]). The transformation of the state space model is done with a similarity transform matrix T_t. This matrix can be determined by calculating the solution Q from the observability Gramian of the full state space system $A_s^T Q A_s + C_s^T C_s = Q$, by decomposing this solution ($Q = T_q T_q^T$) and calculating $T_t = T_q^{-T}$. The state matrices in output normal form can be calculated with $A_T = T_t A T_t^{-1}$, $B_T = T_t B$, $C_T = C T_t^{-1}$ and $D_T = D$. When these transformations are done, the columns of the matrix $\begin{bmatrix} C_T \\ A_T \end{bmatrix}$ are orthogonal. A second similarity transformation is done to transform the matrix to a Hessenberg form (the needed transformation matrix can be calculated with Given's rotations or Householder transformations). The resulting matrix $\begin{bmatrix} C_H \\ A_H \end{bmatrix}$ now can be decomposed with the following parameterization:

$$\begin{bmatrix} C_H \\ A_H \end{bmatrix} = T_1(\beta(1)) .... T_n(\beta(n)) \begin{bmatrix} 0 \\ I_n \end{bmatrix}. \tag{32}$$

In this equation $\beta_{AC} = \begin{bmatrix} \beta(1) & \dots & \beta(n) \end{bmatrix}^T$ is a vector with parameters ranging from -1 to 1. and $T_1 .....T_n$ are rotation matrices, see [12]. Ref. [7] describes how these equations can be incorporated in the Kalman filter in fast array form.

4. Results

4.1 Stationary MIMO setup

Subsequent results in this Section are based on Ref. [7]. A MIMO setup as depicted in Fig. 3 was used to analyze the performance of the algorithm for a stationary noise source. The setup has one reference sensor x, two error sensors e_1 and e_2, two secondary sources driven by the control signals u_1 and u_2. At the left hand side a primary noise source U is positioned, which emits a white noise signal. The primary and secondary sources are point, monopole sources. The setup is assumed to be in a free field and there is no feedback from the secondary sources to the reference sensor. A sample frequency of $f_s = 2000$ Hz was chosen. The goal of the system is to minimize the error at sensors e_1 and e_2 by choosing the appropriate filters $\mathbf{W}_{FIR,i}^{(1,1)}(z)$ and $\mathbf{W}_{FIR,i}^{(1,2)}(z)$. A regularization coefficient δ which is nearly optimal was chosen, which means that a fast rate of convergence is achieved without having an overshoot at convergence. The forgetting factor was set equal to $\lambda = 1$. Since a symmetrical setup is used, two identical convergence curves are expected and simulation results show exactly this behavior as can be seen in Fig. 3. The filter is turned on after 1000 samples. The convergence curves of Fig. 3 are the result of averaging 50 simulations.

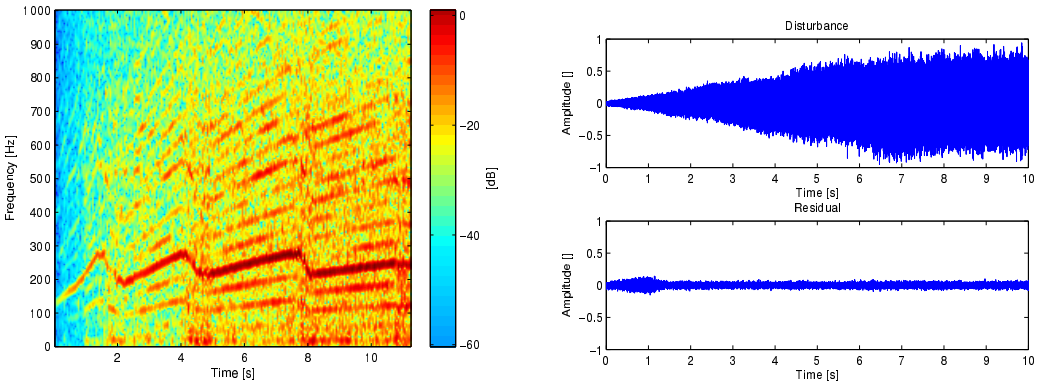

Figure 4: Noise of an acceleration car; Spectrogram (left), disturbance and residual (right) after active control.

4.2 Changing spectrum

The ability of the algorithm to track changes in the spectrum of the noise source was tested with a similar setup, as shown in Fig. 3. An audio file of an accelerating car was chosen as noise source with a varying spectrum as shown in Fig. 4 (left) . The audio-file was filtered with an anti-aliasing filter beforehand, to accommodate for the sampling frequency of $f_s = 2000$ Hz. The algorithm was turned on after 1 second and the result is plotted in Fig. 4 (right). It can be seen that the algorithm has no difficulty with following the changing spectrum.

4.3 Moving noise source

This subsection presents simulation results for a moving noise source, in which the primary path changes. A factor which can reduce the performance of the system is the Doppler effect, which can cause a significant shift in the measured frequency at the reference sensor compared to the error sensors if the noise source velocity is high. The Doppler effect was introduced into the simulations with the equations as shown in Ref. [14]. The robustness of the SISO version of the algorithm to secondary path modeling errors is already investigated by Ref. [5]. The other non-stationarities were tested in separate simulations. For simplicity a SISO setup was used in free field conditions, as shown in Ref. [7].

4.4 Tracking behavior of primary path changes

The influence of a changing primary path was tested with the following simulation: A noise source was assumed to be moving along the y-axis whereas the error sensor and secondary source had fixed positions on the y-axis. A reference sensor was co-located with the noise source. This setup gives a constant secondary path, but a changing primary path. The velocity was set at $v = 0.01\ m/s$, so that a negligible Doppler shift occurs. In Fig. 5 the results are plotted for a white noise source. The filter is turned on after 0.5 seconds. After filter convergence the residual signal becomes progressively larger as function of time. It can be concluded that the filter has a poor tracking performance. Since the filter estimation part has been formulated as an exponentially weighted recursive least squares filter to increase tracking, a forgetting factor lower than one was tried.

Although an improvement in tracking was achieved, the algorithm becomes unstable after a number of iterations depending on the value of λ. This is shown in the upper part of Fig. 5. Instabilities were also observed when a forgetting factor is used in Eq. (30). These instability problems are known for the exponentially weighted fast RLS algorithms, but although some suggestions for improving the numerical behavior are done in Refs. [15–17] unfortunately no solutions preventing instability for the fast array RLS form are known as of yet. Sayed[16] suggests that possible numerical problems occur in the hyperbolic rotation, needed for calculation of Θ_{i-1}. Multiple implementations for calculating the transformation matrix have been tried, including one Householder transformation, a combination of a circular

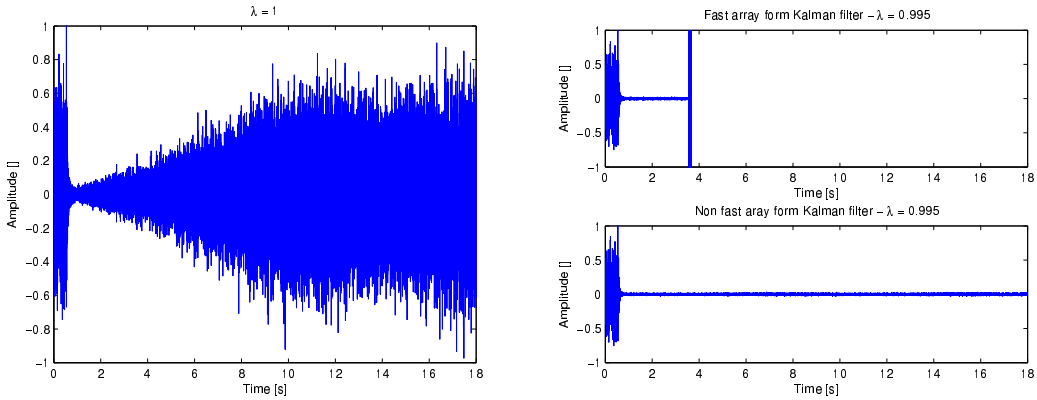

Figure 5: Noise source moving at $v = 0.01\ m/s$, the filter is turned on after 0.5 seconds. Left figure: $\lambda = 1$. Right figure: $\lambda = 0.995$; The upper part of the figure on the right shows the unstable behavior of the fast array form of the Kalman filter. The lower part on the right shows the performance of the same Kalman filter without the built in shift-invariance and here the instability does not occur.

Givens rotation with a hyperbolic Givens rotation, and the orthogonal diagonal method. It was observed that all these variants have different numerical behavior, but the instability occurs with every method. For comparison the array version of the Kalman filter without the built-in shift-invariance property was tried[16]. This algorithm uses only circular transformations, and it was found that the algorithm does not suffer from the mentioned instability, as shown in the lower part of Fig. 5, but it needs significantly more arithmetic operations per iteration, making it less suitable for real-time implementations.

4.5 Experimental results

A SISO version of the algorithm was implemented on a Real Time Linux platform, of which the details can be found in Ref. [18]. The algorithm was tested in an experiment in which the goal was to minimize the acoustic pressure at the right hand side of a duct, caused by a white noise source on the left hand side of a duct. The duct has a length of 3.10 m. At 45 cm from the end of the duct a secondary noise source was placed. The duct was placed in a lab environment of dimensions $4.50 \times 5.20 \times 3.50$ m. At the end of the pipe a microphone was placed and a digital reference signal was used, which is the same signal driving the white noise source at the end of the duct, so that no feedback from the secondary loudspeaker to the reference signal occurs. A sample rate of $f_s = 2000$ Hz was chosen and an FIR filter with $n_w = 150$ filter coefficients was used. The order of the secondary plant model was chosen as $n_s = 30$ and system identification was done off-line with sub-space identification, using SLICOT libraries. The variance accounted for (VAF) values for this order were approximately 99.8%.

4.5.1 Influence of different secondary path models

Implementing the full state space model in the algorithm did not lead to satisfactory results. At a sample rate of 2000 Hz the maximum processing power of the platform was exceeded, so another experiment was done with a sample rate of 500 Hz. At this sample rate the available processing resources were sufficient, but still the algorithm did not work properly. In order to reduce the influence of round-off errors and improve calculation efficiency, an output normal form parameterization, as described in Sec. 3. was used for the state space description of the secondary path. This parameterization resulted in a good working implementation of the algorithm. A sample rate of 2 kHz was used. The convergence curve of an experiment and the power spectral density of the error signal before and after control are shown in Figs. 6. A reduction of the error signal of 14.1 dB was achieved.

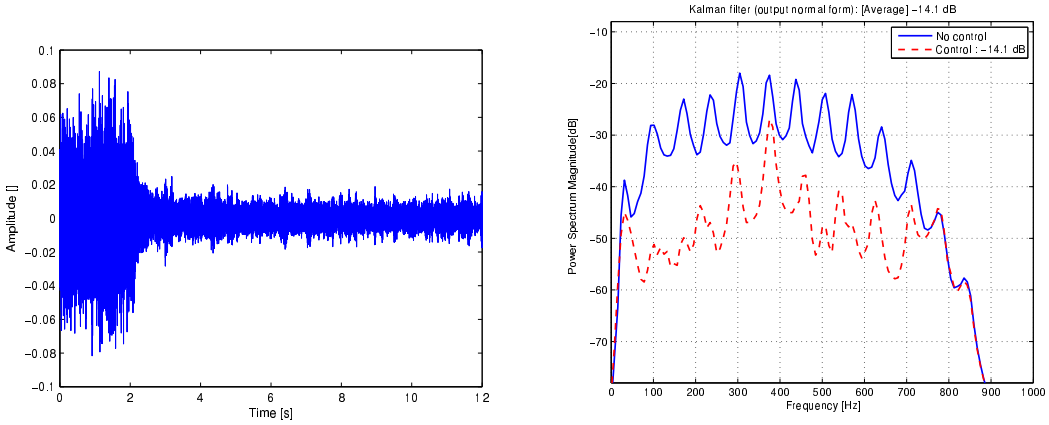

Figure 6: Amplitude measured at the error microphone (left) and power spectral density (right); the filter is turned on after 2 seconds.

4.5.2 Stability

With a forgetting factor of $\lambda = 1$ the algorithm was found to be robust. During experiments the algorithm did not diverge after a running time of a few hours. In these experiments the transformation matrices were calculated with hyperbolic Householder transformations. In experiments with a lower forgetting factor the algorithm, i.e. the fast array version, diverged, which was as expected from the numerical simulations. Other versions of the Kalman algorithm that avoid the numerical issues associated with the non-unity forgetting factors while providing both fast convergence and fast tracking will be published elsewhere [19]

5. Conclusions

Results were shown of a MIMO fast array Kalman filter for use in a feed-forward Active Noise Control system. It was shown how an output normal form parameterization of the secondary path could be implemented effectively into the Kalman filter equations. The performance of the filter was tested in both simulations and in a real-time environment in different noise control setups. It was shown that the filter achieves a good performance in the case of a constant primary path, both with a constant spectrum and a changing spectrum. For a moving noise source, a good tracking performance can be achieved for a forgetting factor lower than unity. In the fast array form of the Kalman filter numerical instabilities are observed for a forgetting factor lower than unity, contrary to the Kalman array form without an incorporated shift-invariance. Numerical results and experimental results correspond well with each other if the estimated secondary path is written in output normal form.

Acknowledgements

The authors would like to thank Geert Jan Laanstra and Henny Kuipers of University of Twente, Signals and Systems group.

References

1. S.J. Elliott. *Signal Processing for Active Control*. Academic Press, 2001.
2. E. Bjarnason. Active noise cancellation using a modified form of the filtered-x LMS algorithm. *Proc. of Eusipco 92, 6th Europ. Sign. Proc. Conf.*, pages 1053–1056, 1992.
3. S.J. Flockton. Fast adaption algorithms in active noise control. *Sec. Conf. on Rec. Advanc. in Act. Noise Contr. of Sound and Vibr.*, pages 802–810, Apr. 1993.

4. A.H. Sayed and T. Kailath. A state space approach to adaptive RLS filtering. *IEEE Sign. Process. Mag.*, pages 18–60, 1994.
5. R. Fraanje. *Robust and Fast Schemes in Broadband Active Noise and Vibration Control*. PhD thesis, University of Twente, 2004.
6. S. van Ophem and A.P. Berkhoff. Real-time Kalman filter implementation for active feedforward control of time-varying broadband noise and vibrations. In *Proc. ISMA 2012*, pages 1–12. KU Leuven, 2012.
7. S. van Ophem and A.P. Berkhoff. Multi-channel Kalman filters for active noise control. *J. Acoust. Soc. Am.*, pages 2105–2115, 2013.
8. K. Zhou, J. C. Doyle, and K. Glover. *Robust and Optimal Control*. Prentice Hall, Upper Saddle River, New Jersey 07458, 1996.
9. B. Sayyarrodsari, J.P. How, B. Hassabi, and Alain Carrier. Estimation-based synthesis of H_∞-optimal adaptive FIR filters for filtered-LMS problems. *IEEE Trans. on Sign. Process.*, 49.NO.1:164–178, 2001.
10. S. van Ophem and A.P. Berkhoff. Performance of a multi-channel adaptive kalman algorithm for active noise control of non-stationary sources. In *Proc. Internoise 2012*. INCE, 2012.
11. A.H. Sayed. *Fundamentals of Adaptive Filtering*. John Wiley & Sons Inc., 2003.
12. M. Verhaegen and V. Verdult. *Filtering and System Identification: A least Squares Approach*. Cambridge University Press, 2007.
13. R. A. Roberts and C. T. Mullis. *Digital Signal Processing*. Addison-Wesley, 1987.
14. A.P. Dowling and J.E. FFowcs Williams. *Sound and Sources of Sound*. John Wiley & Sons, 1983.
15. A. W. Bojanczyk and A. O. Steinhardt. Stabilized hyperbolic householder transformations.
16. A. H. Sayed. *Fundamentals of Adaptive Filtering*.
17. K. Hencke T. K. Moon and J. H. Gunther. An approach to stabilizing the fast array RLS adaptive filter using homogeneous coordinates in projective geometry. In *Proc. Asilomar Conf. on Sign., Syst. and Comp.*
18. J. M. Wesselink. *A rapid prototyping system for broadband multichannel active noise and vibration control*. PhD thesis, University of Twente, 2009.
19. S. van Ophem and A.P. Berkhoff. to be submitted, 2013.